Chapter 4
Materials for the Nuclear Energy Sector

Michael Law, David G. Carr and Sven C. Vogel

Abstract Current and future nuclear-technologies such as fission and fusion reactor-systems depend on well-characterized structural materials, underpinned by reliable material-models. The response of the material must be understood with science-based models, under operating and accident conditions which include irradiation, high temperature and stress, corrosive environments, and magnetic fields. Neutron beams offer methods of characterizing and understanding the effects of radiation on material behaviour such as yield and tensile strength, toughness, embrittlement, fatigue and corrosion resistance. Neutron-analysis techniques improve our understanding of radiation damage, which is essential in guiding the development of new materials.

4.1 Introduction

Radiation damage changes structural materials; the role of microstructure, stress, and radiation flux on swelling, creep, embrittlement, and phase transformations must all be understood. This knowledge will allow development of materials with superior resistance to fast-neutron fluence and high temperatures.

The ability to model and predict the performance and life of materials in nuclear power plants is essential for the reliability and safety of these technologies. These systems may include new environments such as high-pressure water, molten salt, molten metal, and helium which all increase the potential for material degradation

M. Law (✉) · D.G. Carr
Australian Nuclear Science and Technology Organisation, Lucas Heights, NSW, Australia
e-mail: michael.law@ansto.gov.au

D.G. Carr
e-mail: david.carr@ansto.gov.au

S.C. Vogel
Los Alamos National Laboratories, Los Alamos, MN, United States
e-mail: sven@lanl.gov

G.J. Kearley and V.K. Peterson (eds.), *Neutron Applications in Materials for Energy*, Neutron Scattering Applications and Techniques,
DOI 10.1007/978-3-319-06656-1_4

and corrosion. Significant material-development challenges must be met as components of Generation IV reactor systems will experience higher fluxes, temperatures, and sometimes stresses, than conventional light-water reactor systems. The same applies for fusion reactors which in the current developmental phase pose significant challenges to available structural materials. Only by improved characterization can we move to science-based models of material behaviour. Understanding material behaviour from the atomic level up to the full-component scale is essential in developing new materials for these applications.

Creep and creep-fatigue of reactor materials is poorly understood. When the effects of irradiation are added, it is obvious that a better understanding is required. These same effects are intensified in welds due to texture, material inhomogeneity, residual stress, and thermal-expansion mismatch.

Irradiation can cause significant microstructural changes including atomic displacement, helium bubble formation, irradiation-induced swelling and irradiation-induced creep, crystalline-to-amorphous phase transitions, and the generation of point defects or solute aggregates in crystalline lattices. Irradiation also creates defects resulting from atomic displacement or from transmutation products. These defects increase the yield and tensile strengths while reducing ductility and causing embrittlement.

The neutron-beam techniques relevant to the nuclear-energy sector are residual stress and texture measurements, crystallographic phase analysis to establish phase diagrams and reaction kinetics, neutron radiography and tomography, prompt-gamma activation analysis, and small-angle neutron scattering. As exposure to neutron beams activates many materials, neutron facilities generally have the infrastructure to accommodate radioactive materials which allows post-irradiation examination of samples.

The ability to characterize materials in situ is essential, at the appropriate temperature and environment, rather than bringing the sample back to ambient conditions. This also allows the evolution of material behaviour to be studied rather than just the properties at the start and endpoint.

4.2 Steels

Steels are important structural materials in modern nuclear-power systems. Common alloy systems include ferritic materials which have high resistance to radiation induced swelling, nickel-based alloys for high-temperature applications, and austenitic (stainless) steels which typically offer superior corrosion resistance. Typical applications are piping, pressure vessels, heat exchangers, steam generators, and general structural components. Some reactor vessels are made from a ferritic shell which is then clad with stainless steel for corrosion resistance. Structural integrity issues which have been investigated by neutron methods include stress corrosion cracking, weld and cladding cracking, and loss of creep strength and embrittlement due to exposure to temperature and radiation.

Hydrogen can be absorbed into metals, particularly at high temperatures. This interstitial hydrogen can significantly affect the strength and ductility of the material, leading to reduced structural integrity. Hydrogen flows along gradients of interstitial spacing, particularly the variations caused by temperature and stress. Thus it will flow to hot areas associated with welding, and to stress concentrations associated with crack tips. As a strong incoherent scatterer of neutrons, the hydrogen distribution in metals can be investigated with radiography and prompt-gamma neutron activation analysis.

A new class of steels, the oxide-dispersion strengthened steels, have recently been developed specifically for improved radiation tolerance. This material contains a fine dispersion of nano-sized, precipitate-like features which improve high-temperature creep properties and act as sinks for transmutation-produced helium, provide better void-swelling resistance and promote recombination of irradiation-induced point defects. Small-angle neutron scattering has proved to be a particularly useful technique for bulk characterisation of the nano-cluster distribution, volume fraction, shape, interface and size.

4.2.1 Residual Stress

Residual stresses are those that remain in a component after external forces are removed; they are self-equilibrating in nature and are often caused by deformation or uneven heating during manufacture; particularly casting, forging, forming, or welding operations. Residual stresses are significant in the failure of components as they contribute to fracture, fatigue, stress corrosion cracking (SCC), hydrogen-assisted cold cracking, hydride formation, or lead to unacceptable deformation during manufacture. An understanding of residual stress is essential in developing new components, materials, and joining techniques for nuclear-energy systems.

As most metal-forming operations involve heating and or deformation, residual stresses are almost always present due to differential thermal-strains, phase transformations, or plastic mismatch. These mismatches cause elastic strains, which result in residual stresses. The structural issues that arise from residual stresses are of two types, those that are conventional structural-integrity issues (fracture, fatigue, stress corrosion cracking susceptibility, creep crack growth, hydride formation, and distortion) and issues that come about due to the interaction of residual stress and radiation with service exposure (stress relaxation, creep, and swelling; all induced by radiation).

Structural integrity assessments of nuclear components rely on accurate values of the residual stresses; in the absence of better information these must be conservatively assumed to be equal to the yield strength, leading to small critical-defect sizes and loads. The regular use of residual stress measurements by neutron diffraction has been able to safely reduce the conservatism of these estimates by providing accurate, validated measurements. Stresses cannot be measured directly, only the elastic strains locked into the material. Broadly speaking, there are two

methods of measuring residual stresses; compliance methods and methods that measure lattice strains in crystalline materials (typically metals) [1–3]. Compliance methods assess deformations that occur during cutting or other methods of material removal. Lattice strains are typically measured by diffraction and comparing lattice spacings in the strained and unstrained condition, this can be done by X-ray (including synchrotron) and neutron diffraction. Neutron diffraction has many advantages over other methods of measuring residual stresses due to its good penetrating power and spatial resolution within the bulk of the component.

A difficulty with diffraction measurements is that a stress-free sample is often required for reference. Furthermore, the compositional strain-variation that may occur across welds leads to unavoidable sources of error due to so-called chemical strains. There may be significant variation in the weld position and composition between the stress-free sample and the measured component. Where one stress component is known to be near zero measurement at a range of angles normal to the surface using the $\sin^2\theta$ technique [3] can obviate the need for a stress-free sample.

4.2.1.1 Welding and Joining

Welds are often located at mechanical-stress concentrations, and welds can be regarded as a form of metallurgical notch due to degraded local material properties, defects, and residual stresses. The combination of high stresses, reduced material properties, and probable defects often leads to failure by fracture, fatigue, stress corrosion cracking, or even creep cavitation.

Although developing materials for demanding applications is essential, joining these materials will be a major difficulty. Welds and other methods of joining are inevitably the weak point due to metallurgical inhomogeneity, defects, residual stresses, and dissimilar mechanical properties. Well-characterized residual stresses are essential for assessing the structural integrity of welds. In a similar manner to the stress redistribution that may occur with high temperature, irradiation can change the residual stress distribution in the weld (Fig. 4.1).

Residual stresses may occur between layers in composites such as the commonly-used austenitic (stainless steel) cladding on ferritic pressure vessels (Fig. 4.2). These layered composites have two forms of stress, any residual stress due to the bonding process, and a thermal mismatch which is a function of the different coefficients of thermal expansion, and the difference between the bonding temperature and the current (measurement or operational) temperature. In some cases the cladding is too thin for residual stress measurements and only the residual stresses in the base material can be measured [5].

The welds and heat-affected zones (HAZs) are areas of concern for SCC because of the presence of as-fabricated flaws, high residual stresses, elevated plastic strains, chemical heterogeneity, and microstructural differences relative to base metals. Dissimilar metal welds are critical areas in nuclear-power systems due to higher residual stresses than for similar-metal welds, and additional thermal stresses during operation due the different coefficients of thermal expansion.

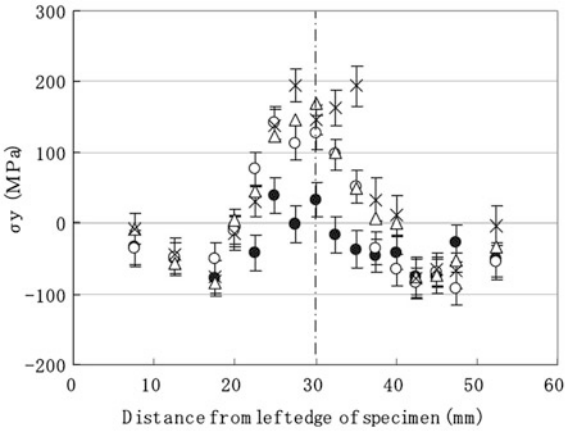

Fig. 4.1 Comparison of residual stress distributions in stages of irradiation (Reprinted with permission from (Y. Ishiyama, R.B. Rogge, M. Obata, J. Nucl. Mater. **408**, 153 (2011)) [4]. Copyright (2011) Elsevier

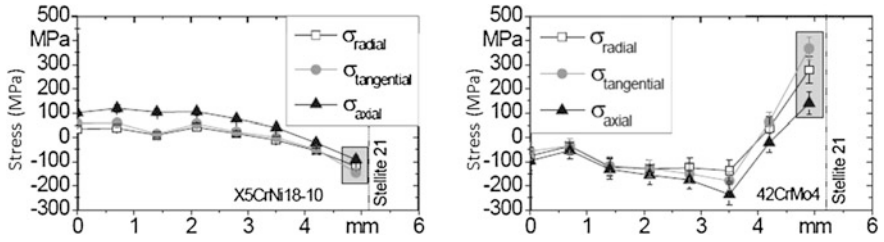

Fig. 4.2 Residual stresses in base material only in Stellite-clad steel specimens. Reprinted with permission from (H. Köhler, K. Partes, J.R. Kornmeier, F. Vollertsen, Phys. Procedia **39**, 354 (2012)) [5]. Copyright (2012) Elsevier

Many of the materials of interest for nuclear-power systems are difficult for neutron diffraction due to large grain size in the weld (stainless steels, U, Zr), low scattering (Zr, Ti), or strong attenuation (W). Hexagonal and orthorhombic crystal structures (Ur, Zr) can complicate residual stress measurement due to type II (inter-granular) stresses from elastic, thermal, and plastic anisotropy which are superimposed on the type I macroscopic stresses.

Dissimilar metal welds (austenitic to ferritic) or bonding system (e.g. copper-tungsten composites for the plasma facing component in fusion systems) requires measurement of different reflections necessitating a different instrument configuration for each material.

Inevitably components will need to be modified or repaired and weld repairs complicate an already complex residual stress field. Repair welds are of special interest as they are often made without post-weld heat treatment, producing welds with higher levels of residual stress (and sometimes hydrogen) than conventional welds. Nearly

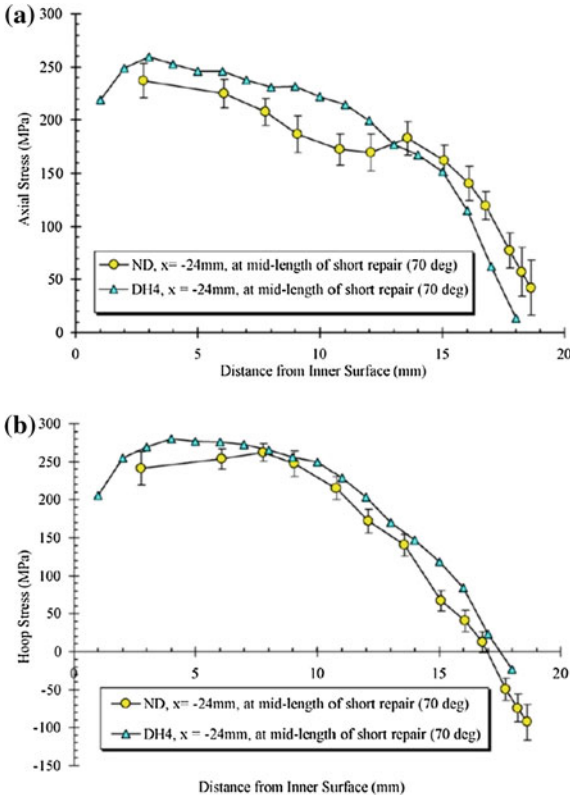

Fig. 4.3 Comparison of measured residual stresses in the HAZ of a short repair weld: **a** axial, **b** hoop. Reprinted with permission from (P. J. Bouchard, D. George, J.R. Santisteban, G. Bruno, M. Dutta, L. Edwards, E. Kingston, M. Smith, Int. J. Press. Vessels Pip. **82**, 299 (2005)) [7]. Copyright (2005) Elsevier

half of repair welds made on high-energy components in the power-generation industry subsequently fail. Repair welds are more complex than normal fabrication welds as the repair may have significant stop/start thermal fields, may possess further transformation stresses, and overlay an existing residual stress field. Edwards et al. [6] and Bouchard et al. [7] made neutron-diffraction measurements of residual stresses in typical repair welds for the nuclear industry. Figure 4.3 shows a good comparison between residual stresses measured by deep hole drilling and by neutron diffraction for a short weld-repair in a 20 mm thick 316 stainless vessel.

4.2.1.2 Measurement Validation

Due to experimental uncertainties, there is considerable variation in residual stress measurements; a common strategy is to validate measurements by using two or more methods. Some neutron residual stress measurements have been validated (Figs. 4.4 and 4.5) by modelling [8], deep hole drilling [7], or contour methods [8, 9].

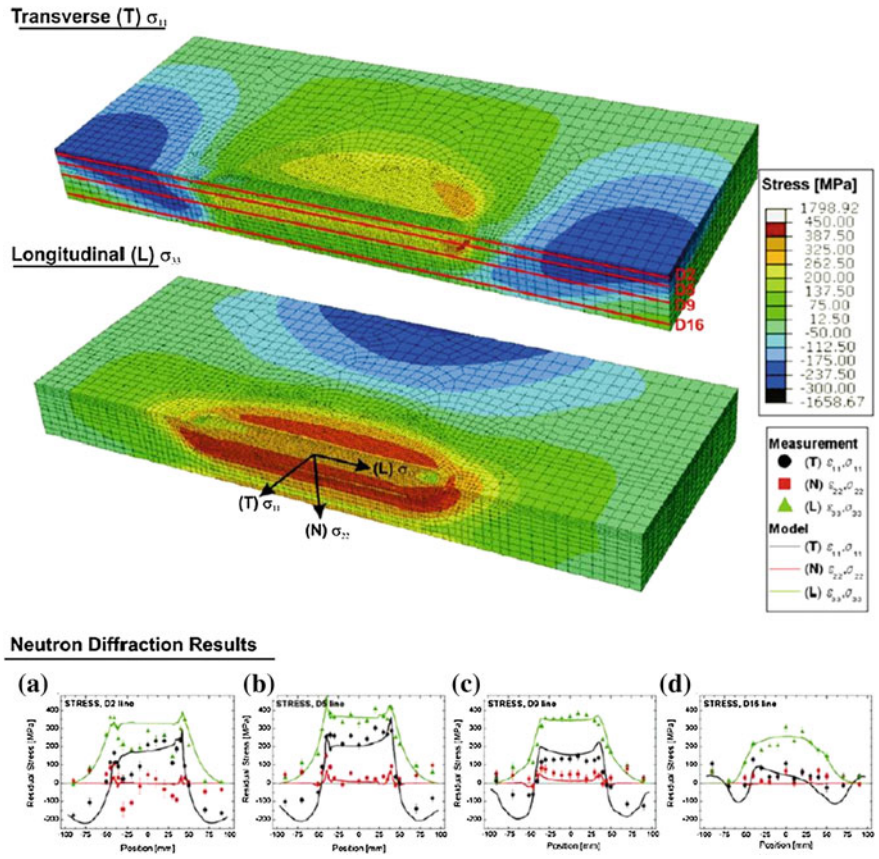

Fig. 4.4 Comparison of model and neutron diffraction measurements. Contour plots of predicted transverse ($\sigma 11$) and longitudinal ($\sigma 33$) residual stresses. Predicted stresses compared with (**a**–**d**) neutron diffraction-measured residual stresses along the *D lines*. Reprinted with permission from (O. Muránsky, M.C. Smith, P.J. Bendeich, T.M. Holden, V. Luzin, R.V. Martins, L. Edwards, Int. J. Solids Struct. **49**, 1045 (2012)) [9]. Copyright (2012) Elsevier

Due to the time and complexity of residual stress measurements, computer modelling of residual stresses has been pursued by many groups. The development and validation of models relies heavily on residual stress measurements. As there are significant uncertainties in both modeling and in residual stress measurements, the two activities inform each other's results. Agreement between modelling and measurements, or between different measurement techniques, improves confidence in both sets of results.

The Versailles Project on Advanced Materials and Standards (VAMAS) Technical Working Area (TWA) 20 ring-and-plug strain round-robin specimen has been used to validate neutron diffraction measurements with good correspondence in results [11].

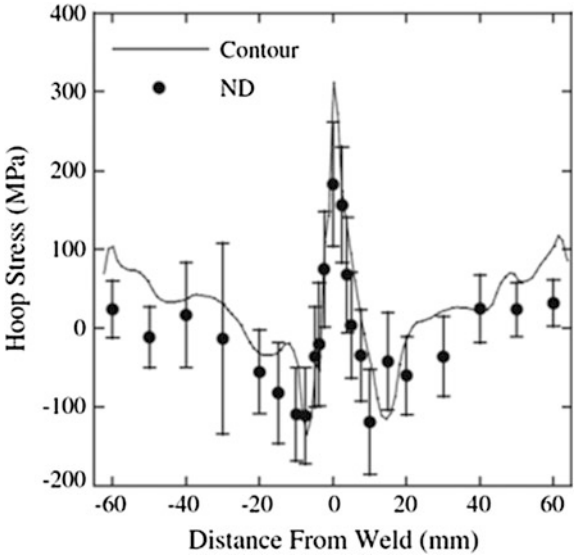

Fig. 4.5 Hoop residual stresses in E-beam welded uranium cylinder measured by *neutron diffraction* and by the *contour method*. Reprinted with permission from (D.W. Brown, T.M. Holden, B. Clausen, M.B. Prime, T.A. Sisneros, H. Swenson, J. Vaja, Acta Mater **59**, 864 (2011)) [10]. Copyright (2011) Elsevier

The European network on neutron techniques standardization for structural integrity (NeT) round robin had a number of samples for both residual stress measurement (by neutron diffraction, with some deep hole drilling and also using the contour method) and modelling [12–15]. The results show good correspondence (Fig. 4.6), although there were some systematic shifts in modelling and contour-method results, when compared to other methods. This led to changes in material descriptions used in modelling, and an appreciation of the effects of localized yielding on contour-method results during cutting.

There are difficulties comparing results as the neutron method averages stresses within the gauge volume. Finite-element analysis (FEA) results are discrete so the results should be volume-averaged to produce values over similar gauge volumes to neutron diffraction results. As real welds often have significant distortion, the spatial position of neutron results should be considered, if they were taken in a straight line they will often be at different distances from the surface while FEA results made on a ‘straight’ weld will be from different areas.

4.2.2 Nano-Particle Strengthening

Modern steels are strengthened by finely dispersed nano-particulates, particularly in high-temperature structural materials. Radiation damage and temperature can cause these to change their shape, size, and distribution, leading to embrittlement. Oxide dispersion strengthened (ODS) steels are designed for high-temperature operation; they contain oxide nano-clusters (e.g. yttrium-titanium oxide) in a ferritic-steel matrix.

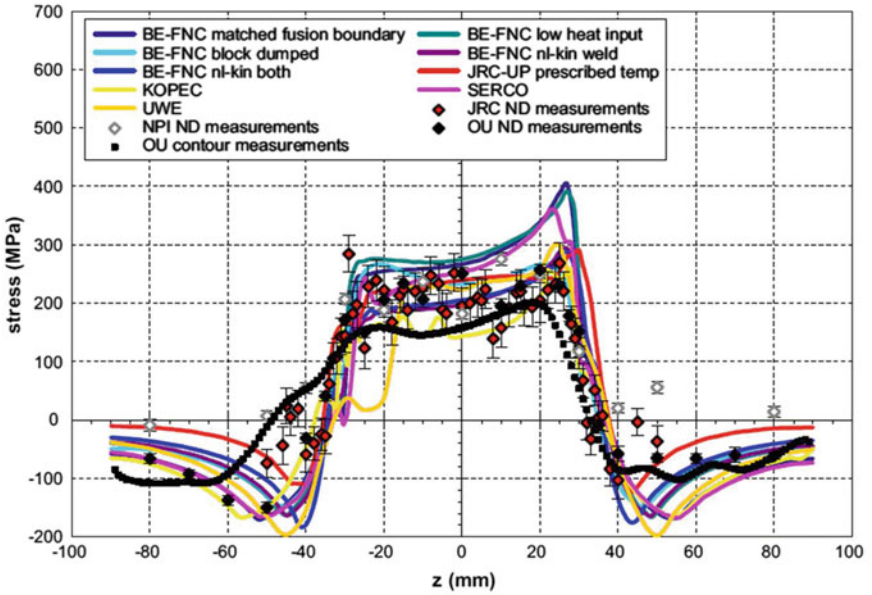

Fig. 4.6 Comparison of modelling predictions and neutron diffraction and contour method measurements for the NeT task group 1 single weld-bead on plate. Reprinted with permission from (M.C. Smith, A.C. Smith, Int. J. Press. Vessels Pip. **86**, 79 (2009)) [13]. Copyright (2009) Elsevier

The size and morphology of these particles may change with exposure to stress, temperature, or radiation; all conditions which occur in nuclear-power systems, typically increasing the size and decreasing the number of strengthening particles. Changes in the volume fraction, surface interface and size distribution of these particles can cause significant changes to the strength, ductility, and toughness of these materials. Advanced reactor-materials use nano-particulates to act as sinks for radiation-induced phenomena such as vacancies, self-interstitials, and as trapping sites for He bubbles from nuclear reactions in the material. Small-angle neutron scattering (SANS) can non-destructively analyse these nanoscale features over a large sample volume.

The use of a strong magnetic field can differentiate between magnetic and non-magnetic scattering at right angles to each other, and the strengthening nano-particulate oxides are typically non-magnetic. With ODS steel samples the SANS curves for no magnetic field (nuclear scattering only) and with field (nuclear + magnetic scattering) are compared. If they have no difference then the scattering is entirely non-magnetic and it can be assumed that the scattering is from the non-magnetic oxide nano-clusters. If there is a difference then the contribution from iron-based magnetic scatterers can be removed. This experimental technique should be used in conjunction with an oxide-free reference sample of the same manufacturing route (if possible), for correct de-convolution of the SANS from oxide nano-clusters.

The size of strengthening nano-particles is in the range 1–20 nm, and the few techniques available for studying these are transmission-electron microscopy (TEM), atom-probe tomography (APT), and SANS, however TEM and APT only sample a small volume. As a result, SANS has become a critically important technique for the development, understanding and characterisation of these irradiation-resistant materials [16, 17].

4.3 Zirconium and Its Alloys

Zirconium and its alloys are extensively used in nuclear applications due to the combination of a low neutron-absorption cross section, good mechanical properties under high stress and temperature conditions, low hydrogen/deuterium uptake and corrosion resistance. The main uses are for some structural components (particularly the calandria in CANada Deuterium Uranium (CANDU)-type reactors) and fuel cladding. It is anticipated to be used in the primary containment-vessel of high temperature D_2O inside the core of the fourth generation supercritical-water-cooled reactor (SCWR). Its behaviour during manufacturing and in service as well as under accident scenarios is therefore of great importance and a topic of extensive research.

Pure zirconium has a hexagonal closed-packed (hcp) crystal structure up to 866 °C and transforms to a body-centred cubic (bcc) crystal structure at higher temperatures. Their complex deformation-mechanisms have been investigated with neutron diffraction where different crystallographic planes have different elastic constants and post-yield behaviour, leading to strain partitioning. The main alloying elements for nuclear applications are niobium and tin, the latter forming together with other minor elements the so-called Zircaloys (*Zircaloy is a trademark of Westinghouse Electric Company, Pittsburgh, PA.).

Neutron diffraction has been applied to zirconium and its alloys to characterize welds, as an in situ mechanical test technique to characterize deformation modes to allow predictive modelling of deformation, to investigate the development of texture under temperature and stress, and to characterize the phase transformations including texture-variant selection during the hcp/bcc phase transformation. The following sections describe some of these experiments.

Zircaloys are also prone to brittle-hydride formation, particularly in welds. Hydrides can also form in parent plate if unfavourable textures are present due to a particular manufacturing route. Thus, many investigations have been performed on hydrides, such as imaging their location (radiography and prompt gamma), and assessing their susceptibility to hydride formation (residual stress and texture). Hydrogen accumulation or “pick-up” can also occur in the Zircaloy cladding of nuclear fuel and can cause embrittlement. In this case, the hydrogen content can be spatially visualized and quantified by neutron radiography. Blistering of Zircaloy fuel-cladding has also been investigated using neutron radiography, as X-rays are not effective in practice due to the high background, which includes gamma radiation from decay products.

4.3.1 Deformation

Due to the complex deformation behaviour of highly-anisotropic Zirconium alloys, these materials have been studied extensively by neutron diffraction, in combination with polycrystalline deformation models, the elasto-plastic and visco-plastic self-consistent models [18], to understand the deformation and texture development.

The difference in tensile and compressive behaviour in Zircaloy-2 was demonstrated by MacEwen et al. [19]. The strains were measured for each lattice plane on a time-of-flight (TOF) instrument (the General Purpose Powder Diffractometer at the intense-pulsed neutron source (IPNS), which is no longer operational). Neutron time-of-flight instruments can measure multiple lattice planes without reorienting the sample, as is required on a constant-wavelength instrument.

The residual stresses, stress tensor, and inter-granular stresses were characterized after 5 % strain by Pang et al. [20]. The measured lattice strains were in good agreement with those predicted by elasto-plastic self-consistent models, which predict deformation modes such as slip and twinning.

Zirconium and its alloys have a hcp structure, and there are too few slip systems for standard plasticity so twinning is an important contributor to plastic deformation. Rangaswamy et al. [21] compared changes in texture and twin volume-fractions to predictions from a visco-plastic self-consistent polycrystal model, which described both slip and twinning.

Balogh et al. [22] examined the deformation behaviour of Zr-2.5Nb samples by full-pattern diffraction line-profile analysis (DLPA) to determine the evolution of the density and type of the dislocation-structure induced by irradiation and plasticity. Control samples were compared to samples removed from a CANDU nuclear reactor pressure-tube to determine the evolution of microstructure and plasticity characteristics during deformation (27 % cold work during manufacture). The pressure tube was in service for 7 years at $\sim$250 °C with a neutron fluence of $1.6 \times 1024\ m^{-2}$ (E > 1 MeV). Results show that fast-neutron irradiation significantly increases the overall dislocation density, accomplished entirely by an increase in the $\langle a \rangle$ Burgers vector dislocations.

4.3.2 Residual Stress

Welding is commonly used to fabricate zirconium-alloy components. Welding commonly results in residual stresses, and these can be complex due to the anisotropy of the material. Residual stresses can lead to hydride formation, so are significant to the structural integrity of the material. Using time-of-flight neutron diffraction, Carr et al. [23, 24] measured the residual stresses (Fig. 4.7) in a Zircaloy-4 gas tungsten arc weld. They also determined the lattice strains, texture, and the strain evolution in the weld during loading.

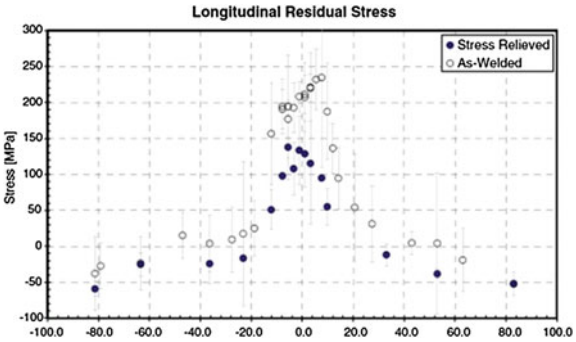

Fig. 4.7 Variation of the macroscopic residual-stresses in a Zircaloy-4 weld after a stress-relieving heat-treatment (*filled circles*) and as-welded (*open circles*). The as-welded stresses are reduced by about 40 % by the heat treatment. Measurements were taken across the plate at the mid-thickness position. Reprinted with permission from (D.G. Carr, M.I. Ripley, D.W. Brown, S.C. Vogel, T.M. Holden, J. Nucl. Mat. **359**, 202 (2006)) [24]. Copyright (2006) Elsevier

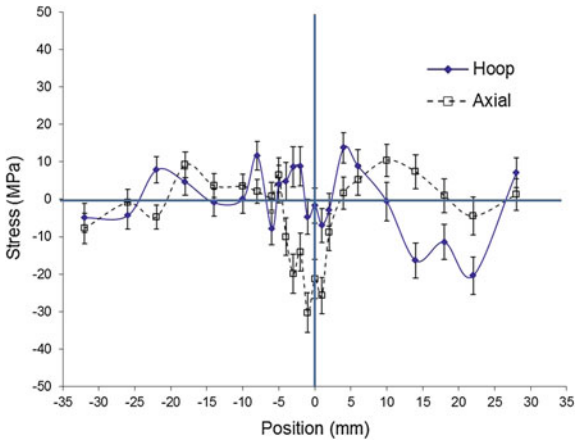

Fig. 4.8 Residual stresses in Zircaloy weld. Reprinted with permission from (P. Bendeich, V. Luzin, M. Law, Australian Nuclear Science and Technology Organisation report (2012)) [25]

Welding often leads to grain growth and crystallographic texture changes, which may result in limited numbers of crystals which satisfy the diffraction condition, leading to poor statistics and errors. Methods of overcoming this include increasing the sampled area by increasing the gauge volume, and rocking or sweeping the sample through a larger volume. The residual stresses using such techniques were measured in a girth weld in the Zircaloy containment vessel for a cold-neutron source in a research reactor [25]. The rotational symmetry of the vessel was taken advantage of and the weld was rotated back and forth around the cylinder axis to increase the number of grains sampled. The residual stresses were low (Fig. 4.8) as the weld was subject to post-weld heat treatment to reduce residual stresses and drive off hydrogen trapped in the weld, in an effort to reduce hydrogen cracking and hydride formation.

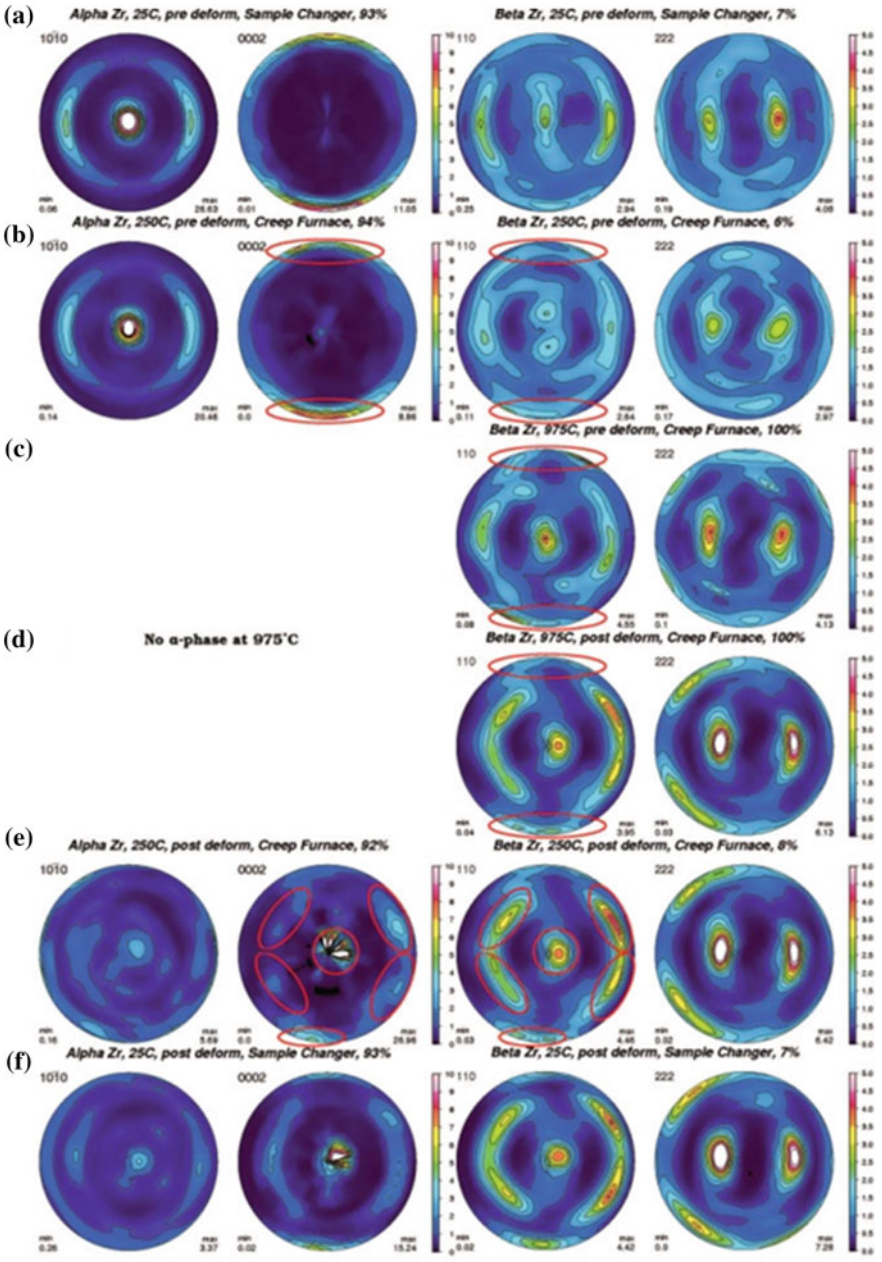

Fig. 4.9 Texture of the α-phase (*left column*) and β-phase (*right column*) of Zr-2.5Nb during heating, with 20 % strain in the axial direction (original extrusion direction), and cooling. The radial direction is *horizontal* on the pole figure and the hoop direction *vertical*. Reprinted from (S.C. Vogel, ISRN Materials Science **2013**, 24 (2013)) [32]

4.3.3 Texture

Texture is the orientation distribution of the single crystals forming the polycrystalline aggregate. Due to the anisotropy of the single crystals, particularly the hexagonal alpha phase, texture is of great importance in the deformation behaviour of zirconium alloys. Therefore, understanding texture evolution during thermo-mechanical processing steps and service is a necessary precursor to predicting texture. Texture is affected by temperature [18, 26] and strain rate [27]. In situ diffraction is essential in understanding texture evolution.

Figure 4.9 shows an example of texture evolution in Zr-2.5Nb, with both temperature changes and deformation. This measurement was made on the HIPPO diffractometer [28, 29] at the Los Alamos Neutron Scattering Center (LANSCE) using a high-temperature deformation furnace [30]. The texture was measured at room temperature and at a number of steps up to 975 °C [31]. At this temperature the sample experienced a compressive strain of 20 %. Texture measurements were made at 975 °C, then at the same temperature steps during cooling to room temperature.

At room temperature the bcc beta phase is meta-stable and increases during heating at locations on the rim of the pole figure where the 0001 alpha pole-figure previously showed maxima, showing that alpha grains transform directly to beta grains [33]. At 975 °C only the bcc beta phase exists, at this point the sample had a strain of 20 %. The beta grains transform to alpha during cooling and (by the Burgers orientation relationship) the {0002} planes of the alpha phase become {110} planes of the beta phase, which is reflected in the texture evolution.

Pre and post treatment conditions of the sample are confirmed in Fig. 4.6a/b and e/f, respectively. The Burger orientation-relationship determines the transition of (0002) hcp/α to maxima in (110) bcc/β during a temperature increase to 975 °C. The resulting textures at high temperature are shown in (c). The (222) bcc/β planes align with the applied compression direction (d). To study the evolution of many properties such as texture, it is necessary to measure at intermediate steps, rather than just the start and end of processing.

Using Bragg-edge transmission [34] and neutron imaging in combination makes simultaneous mapping of the strains and texture (Fig. 4.10) [35] of the crystallites within the entire sample possible.

4.3.4 Zirconium Hydride

Hydride formation in Zircaloys reduces strength and ductility significantly. Hydrides form preferentially in areas of higher stress [36] such as near welds or at crack tips. In loss of coolant accidents (LOCAs), overheated Zircaloy cladding may react with cooling water in a complex manner with different phase-transformation temperatures depending on other species such as oxygen or hydrogen. The solubility of hydrogen in zirconium and Zircaloy differs by almost an order of magnitude between the alpha and beta phases [37], and excess hydrogen may form embrittling hydrides, particularly at

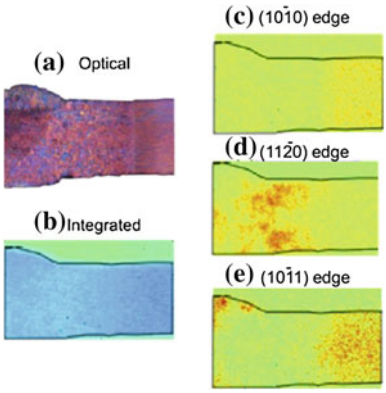

Fig. 4.10 Optical (**a**) and neutron-radiography images (**b**, **c**, **d**, **e**) of the welded Zircaloy-4 plates. Figure **b** was produced using neutrons with wavelengths between 1.4 and 2 Å, whilst Figures **c**, **d** and **e** are images of the height of selected Bragg edges. In figure **c** the start of the HAZ clearly shows the disappearance of the (10–10) Bragg edges, whilst the (11–20) edge in figure **d** reveals the differences between the *outer* and *inner layers* of the plate. Reprinted with permission from (J.R. Santisteban, M.A. Vicente-Alvarez, P. Vizcaino, A.D. Banchik, S.C. Vogel, A.S. Tremsin, J.V. Vallerga, J.B. McPhate, W. Lehmann Kockelmann, J. Nucl. Mater. **425**, 218 (2012)) [35]. Copyright (2012) Elsevier

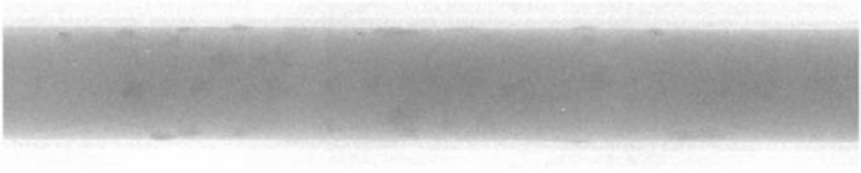

Fig. 4.11 Steel target-rod with Zr cladding after exposure to protons in the target of the Swiss Spallation Neutron Source, SINQ. The *black points* are attributed to the agglomeration of hydrogen on the *inner side* of the Zr cladding. Because the sample is highly activated, a well-shielded facility was used for the investigations. Reprinted with permission from (E.H. Lehmann, P. Vontobel, G. Frei, C. Bronnimann, Nucl. Instrum. Meth. Phys. Res. A **531**, 228 (2004)) [43]. Copyright (2004) Elsevier

crack tips etc. Despite decades of work, the mechanisms of corrosion of zirconium-based alloys, particularly in reactor conditions, are still an active research field.

As hydrogen is a strong neutron-scatterer, the hydrogen concentration (Fig. 4.11) can be measured by neutron radiography [38] with sensitivities of $\sim$1,000 wt. ppm [39]. Neutron diffraction and radiography can be combined [40, 41] to identify and map hydride phases. The distribution [42] and kinetics [37] of hydrogen in materials can be identified by neutron radiography.

The hydrogen concentration in metals (particularly in zirconium-based alloys) can be also be measured by cold neutron prompt-gamma activation analysis PGAA [44]. However, these techniques are not suitable for imaging and rather provide the

bulk average from the volume illuminated by the incident neutron beam. Cold neutron PGAA is based on measuring prompt gamma rays following the absorption of cold neutrons by hydrogen. This method has to be performed in a close proximity to a neutron source. The technique does not change the sample and so is well suited to assessing hydrogen uptake during interrupted corrosion testing.

4.4 Uranium

In this section we describe several applications of neutrons to investigate the crystallography and phase composition of uranium, particularly in fuels. Metallic uranium has an orthorhombic crystal structure, leading to anisotropic single-crystal properties such as a negative thermal-expansion along the crystallographic *b* axis. This leads to substantial integrity problems when the material is heated. Therefore, the vast majority of nuclear fuels in power reactors consist of cubic uranium-oxide whereas in research reactors metallic uranium-molybdenum alloys are also used, with the molybdenum stabilizing the cubic gamma-structure. During operation, i.e. during heating and irradiation, atoms rearrange and phase transformations may occur, with the phases in a spent fuel having different material properties to those of a fresh fuel. For example, thermal gradients of several hundred degrees exist between the centre and outside of a fuel rod, leading to a spatial distribution of crystallographic phases over a distance on the order of a centimeter. The identification of the new phases, determination of their formation conditions and kinetics, as well as establishing their properties, are of paramount importance for new and existing fuel types. Similar considerations apply to structural materials, e.g. cladding or pressure-tubing materials in accident scenarios, and actinide-bearing minerals for mining and waste deposition [45].

In fuels, the elements of interest are high Z-number (uranium and other actinides) and low Z-number (oxygen, nitrogen, carbon). Neutron diffraction is better at determining these structures while X-ray diffraction is biased towards the heavy atoms.

There are three structure models proposed for cubic UC_2 [46–48] a non-quenchable phase existing between ~1,823 and ~2,104 °C [49]. The three crystal structures differ in the arrangement of the carbon atoms. Simulated X-ray diffraction patterns are similar due to the bias towards the uranium lattice. Simulated neutron diffraction patterns can discriminate between the three different structures (Fig. 4.12) due to the sensitivity to the carbon atoms. Experimental neutron-diffraction data matches well with the structure proposed by Bowman [48].

This example illustrates the great advantages neutron diffraction offers over X-ray diffraction for crystal-structure investigations of nuclear materials and in particular nuclear fuels.

The smaller low Z-number elements are typically the mobile species and their rearrangement as a function of temperature leads to phase transitions, and neutron diffraction may be sensitive to these while X-ray diffraction will not. As many phases are non-quenchable, in situ techniques offer great advantages. Classical methods to study phase transitions, such as dilatometry or calorimetry, do not identify the

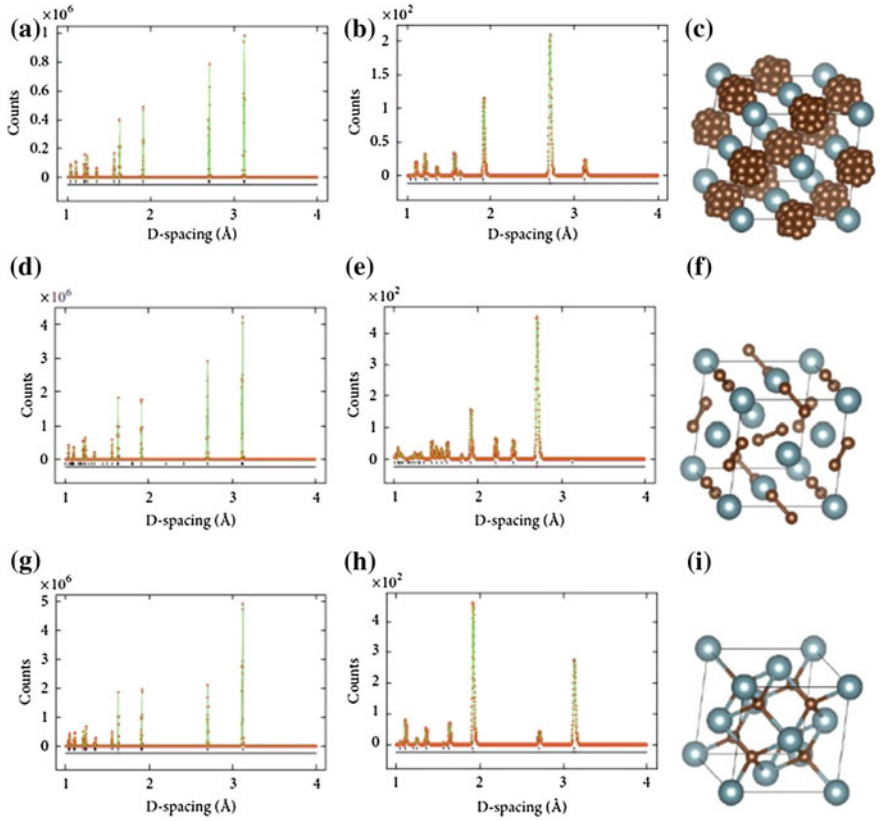

Fig. 4.12 Simulated diffraction patterns for X-rays (*left column*) and neutrons (*right column*) of the three structures for cubic UC_2 proposed by Bowman [48] (*top row*), Bredig [46] (*middle row*), and Wilson [47] (*bottom row*) showing the superiority of neutron diffraction in determining the structure of the cubic UC_2 phase. Reprinted from (S.C Vogel, ISRN Materials Science **2013**, 24 (2013)) [32]

newly-formed phases and are also sensitive to changes in chemical composition, e.g. rearrangement of the oxygen atoms, without formation of a new, distinct phase. Not surprisingly, neutrons have played a vital role over the past decades in elucidating the properties of nuclear fuels.

4.4.1 Structure

Structures of fuels with both light and heavy elements are best determined by neutron diffraction. Urania, with a large range of hyper-stoichiometric oxygen (up to $UO_{2.25}$), has been investigated by neutron diffraction. Many of the phases in the U-O phase diagram were determined by neutron diffraction.

As examples, Willis [50] utilized diffraction from a $UO_{2.13}$ single crystal to establish the positions of the excess oxygen atoms in the CaF_2-type structure; the crystal structure of beta-U_4O_{9-y} was solved by Bevan et al. [51] and later refined by Cooper [52].

Besides Bragg diffraction, where the crystallographic information is derived from the integrated peak intensities via the structure factor, diffuse scattering can be used to study disorder and oxygen diffusion, e.g. Clausen et al. [53], Goff et al. [54]. As the energy of thermal neutrons is similar to the generation or annihilation energies for phonons, neutrons can also be used to probe the lattice dynamics of nuclear materials, e.g. the first phonon–dispersion curve for UO_2 at room temperature measured by Dolling et al. [55]. See also the review article by Hutchings 1987 [56] for a review of earlier neutron scattering work on UO_2 and ThO_2. It is important to stress that the phases and their behaviour has to be studied in situ as the phenomena relevant to operation and accident conditions are temperature controlled.

4.4.2 Kinetics of Phase Transformations

High neutron-flux and improved detectors allow faster data acquisition; if sufficiently fast compared to the reaction rate, in situ kinetic studies are possible. The sensitivity of neutron diffraction to the crystallographic phases and the rate of data acquisition can allow not only the equilibrium state, but any intermediate phases and reaction rates to be determined.

To study the kinetics of phase transformations, hyper-stoichiometric uranium oxide was cycled across a phase boundary [57]. Desgranges et al. [58] performed in situ studies on transitions between four different uranium-oxide phases which depended on both temperature and oxygen partial-pressure. Knowledge of intermediate phases led to a better understanding of the phase-transition process and growth kinetics.

4.4.3 Radiography and Tomography

Neutrons are particularly important in the imaging of nuclear-fuel rods which are strong γ-sources (X-ray background) and are made from heavy metal elements i.e. uranium or lead with a high attenuation of X-rays. A resolution of 50 μm or better can be accomplished and this has been utilized to characterize nuclear materials, e.g. fuel rods [43] or cladding materials [42], see the section on hydrides above. Recent detector developments allowing for spatially and time-resolved neutron detection [59] are likely to open new avenues of characterization of nuclear materials and nuclear fuels in particular as they allow for isotope-sensitive imaging via neutron resonance absorption [60].

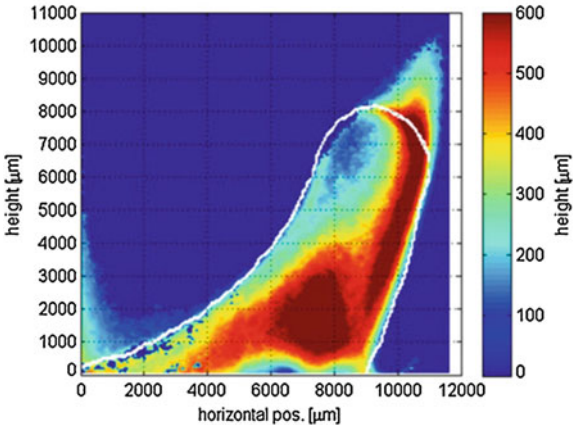

Fig. 4.13 Liquid film thickness on the surface of a vane in a coolant channel. The *white line* is the surface of the vane. Reprinted with permission from (R. Zboray, J. Kickhofel, M. Damsohn, H.M. Prasser, Prasser, Nucl. Eng. Des. **241**, 3201 (2011)) [62]. Copyright (2011) Elsevier

4.5 Coolant

As hydrogen is such a strong scatterer, the presence of hydrogen, water, and hydrides are easily detected in neutron radiography and tomography [61]. Coolant behaviour in the fuel bundle of a boiling-water reactor (BWR) was examined by Zboray et al. [62] with neutron tomography (Fig. 4.13), allowing the coolant flow and channels to be optimized.

4.6 Measurement of Radioactive Samples

Active samples pose additional difficulties; safe handling and sample preparation, transport, shielding, and disposal may all add to the experimental complexity. The standard methods of reducing operator exposure include limiting the amount or size of the sample, increasing the distance from the sample to the operator, limiting exposure time, and the use of shielding [63].

For SANS and texture measurements, the sample size can be favourably small ($\sim$10 mm^3 in some cases). The sample size in radiography is generally defined by the project scope and the scale of the component to be imaged. When measuring residual stresses, reducing the sample size changes the constraint conditions which can significantly alter the measured residual stress; there are simplified methods of assessing the allowable sample size [64]. An additional issue is that reducing sample size by cutting active samples increases operator exposure and leads to active waste. All these factors must be considered for the safe conduct of the

experiment and as well as additional conditions subject to the safety policy of the laboratory. However, in order to understand the real effects of neutron irradiation damage to reactor materials the benefits can sometimes outweigh the complexities involved. By nature, neutron facilities have detailed radiological safety procedures already in place, making the study of radioactive samples perhaps more viable than at other facilities.

4.7 Outlook and Perspectives

Neutron characterization techniques are particularly important in understanding materials for the nuclear-energy sector for many reasons. In structural components the combination of radiography, residual stress, and texture measurements allows assessment of structural integrity and optimization of manufacturing, while SANS provides a unique tool to track the effects of radiation damage. In fuels and waste forms, particularly when heavy and light elements are combined, neutron diffraction has inherent advantages over X-rays.

Neutron characterization techniques will be increasingly important for understanding materials for the nuclear sector. The increased functionality comes partly from new techniques, and partly from improvements in existing techniques.

New techniques such as energy-dispersive neutron radiography and Bragg-edge strain imaging offer new insights into materials. As the technologies are new, large improvements are to be expected in technique and analysis.

Well established techniques will benefit from improvements in neutron flux, detectors, and analysis, enabling in situ or kinetic studies, and smaller samples. Sample environments will increase in complexity to better mimic the studied operating conditions. Shielding or dedicated beamlines will allow characterization of active materials.

Combinations of techniques, such as diffraction and radiography, will provide detailed crystallographic information in combination with a spatially-resolved distribution of the properties of interest.

References

1. P.J. Withers, H.K. Bhadeshia, Mater. Sci. Technol. **17**, 355 (2001)
2. P.J. Withers, H.K. Bhadeshia, Mater. Sci. Technol. **17**, 366 (2001)
3. M.T. Hutchings, P.J. Withers, T.M. Holden, T. Lorentzen, *Introduction to the characterization of residual stress by neutron diffraction* (Taylor & Francis, Boca Raton, 2005)
4. Y. Ishiyama, R.B. Rogge, M. Obata, J Nucl Mater **408**, 153 (2011)
5. H. Köhler, K. Partes, J.R. Kornmeier, F. Vollertsen, Phys. Procedia **39**, 354 (2012)
6. L. Edwards, P.J. Bouchard, M. Dutta, D.Q. Wang, J.R. Santisteban, S. Hiller, M.E. Fitzpatrick, Int. J. Press. Vessels Pip. **82**, 288 (2005)

7. P.J. Bouchard, D. George, J.R. Santisteban, G. Bruno, M. Dutta, L. Edwards, E. Kingston, M. Smith, Int. J. Press. Vessels Pip. **82**, 299 (2005)
8. O. Muránsky, M.C. Smith, P.J. Bendeich, L. Edwards, Comput. Mater. Sci. **50**, 2203 (2011)
9. O. Muránsky, M.C. Smith, P.J. Bendeich, T.M. Holden, V. Luzin, R.V. Martins, L. Edwards, Int. J. Solids Struct. **49**, 1045 (2012)
10. D.W. Brown, T.M. Holden, B. Clausen, M.B. Prime, T.A. Sisneros, H. Swenson, J. Vaja, Acta Mater **59**, 864 (2011)
11. G.A. Webster, J. Wimpory, Mater. Process. Technol. **117**, 395 (2001)
12. C. Ohms, R.C. Wimpory et al., *Residual stress measurements in a three-bead slot weld in a 20 mm carbon steel plate*. PVP2009-77496 ASME Pressure Vessels and Piping Conference, Prague, Czech Republic (2009)
13. M.C. Smith, A.C. Smith, Int. J. Press. Vessels Pip. **86**, 79 (2009)
14. S. Pratihar, M. Turski, L. Edwards, P.J. Bouchard, Int. J. Press. Vessels Pip. **86**, 13 (2009)
15. P.J. Bouchard, Int. J. Press. Vessels Pip. **86**, 31 (2009)
16. G. Albertini, R. Coppola, Nucl. Instrum. Meth. Phys. Res. **A314**, 352 (1992)
17. R. Coppola, F. Fiori, E.A. Little, M. Magnani, J. Nucl. Mater. **245**, 131 (1997)
18. C. Tomé, P. Maudlin, R. Lebensohn, G. Kaschner, Acta Mater. **49**, 3085 (2001)
19. S.R. MacEwen, J. Faber, A.P.L. Turner, Acta Metall. **31**, 657 (1983)
20. J.W.L. Pang, T.M. Holden, P.A. Turner, T.E. Mason, Acta Mater. **47**, 373 (1999)
21. P. Rangaswamy, M. Bourke, D.W. Brown, G.C. Kaschner, R.B. Rogge, M.G. Stout, C.N. Tome, Metall. Mater. Trans. A **33**, 757 (2002)
22. L. Balogh, F. Long, M.R. Daymond, R.A. Holt, D.W. Brown, C.D. Judge, The influence of fast neutron irradiation on the plasticity induced evolution of dislocation densities and operating deformation modes in Zr-2.5Nb, Mecasens, Sydney (2013)
23. D.G. Carr, M.I. Ripley, T.M. Holden, D.W. Brown, S.C. Vogel, Acta Mater. **52**, 4083 (2004)
24. D.G. Carr, M.I. Ripley, D.W. Brown, S.C. Vogel, T.M. Holden, J. Nucl. Mat. **359**, 202 (2006)
25. P. Bendeich, V. Luzin, M. Law, Australian Nuclear Science and Technology Organisation report (2012)
26. G.C. Kaschner, J.F. Bingert, C. Liu, M.L. Lovato, P.J. Maudlin, C.N. Tome, Acta Mater. **49**, 3097 (2001)
27. T.A. Sisneros, D.W. Brown, B. Clausen, D.C. Donati, S. Kabra, W.R. Blumenthal, S.C. Vogel, Mater. Sci. Eng. A **527**, 5181 (2010)
28. H.R. Wenk, L. Lutterotti, S.C. Vogel, Nucl. Instrum. Meth. Phys. Res. A **515**, 575 (2003)
29. S.C. Vogel, C. Hartig, L. Lutterotti, R.B. Von Dreele, H.R. Wenk, D.J. Williams, Powder Diffr. **19**, 65 (2004)
30. H.M. Reiche, Advanced sample environments for in situ neutron diffraction studies of nuclear materials. Ph.D. thesis, New Mexico State University, Las Cruces, New Mexico, U.S.A. (2012)
31. H.M. Reiche, S.C. Vogel, Rev. Sci. Instrum. **81**, 1 (2010)
32. S.C Vogel, ISRN Materials Science **2013**, 24 (2013)
33. D. Bhattacharyya, G.B. Viswanathan, S.C. Vogel, D.J. Williams, V. Venkatesh, H.L. Fraser, Scripta Mater. **54**, 231 (2006)
34. S. Vogel, Ph.D. thesis, Christian-Albrecht-University, Kiel (2000), http://e-diss.uni-kiel.de
35. J.R. Santisteban, M.A. Vicente-Alvarez, P. Vizcaino, A.D. Banchik, S.C. Vogel, A.S. Tremsin, J.V. Vallerga, J.B. McPhate, W. Lehmann Kockelmann, J. Nucl. Mater. **425**, 218 (2012)
36. E. Garlea, H. Choo, G.Y. Wang, P.K. Liaw, B. Clausen, D.W. Brown, J. Park, P.D. Rack, E. Kenik, Metall. Mater. Trans. A **41**, 2816 (2010)
37. M. Grosse, M. Steinbrueck, E. Lehmann, P. Vontobel, Oxid. Met. **70**, 149 (2008)
38. E.H. Lehmann, P. Vontobel, N. Kardjilov, Appl. Radiat. Isot. **61**, 503 (2004)
39. R. Yasuda, M. Nakata, M. Matsubayashi, K. Harada, Y. Hatakeyama, H. Amano, J. Nucl. Mater. **320**, 223 (2003)
40. E. Sváb, G. Mészáros, Z. Somogyvári, M. Balaskó, F. Körösi, Appl. Radiat. Isot. **61**, 471 (2004)

41. A.M. Shaikh, P.R. Vaidya, B.K. Shah, S. Gangotra, K.C. Sahoo, BARC Newsl. **273**, 104 (2006)
42. M. Grosse, G. Kuehne, M. Steinbrueck, E. Lehmann, J. Stuckert, P. Vontobel, J. Phys. Condens. Matter **20**, 104263 (2008)
43. E.H. Lehmann, P. Vontobel, G. Frei, C. Bronnimann, Nucl. Instrum. Meth. Phys. Res. A **531**, 228 (2004)
44. A. Couet, A.T. Motta, R.J. Comstock, R.L. Paul, J. Nucl. Mater. **425**, 211 (2012)
45. P.C. Burns, R.C. Ewing, A. Navrotsky, Science **335**, 1184 (2012)
46. M.A. Bredig, J. Am. Ceram. Soc. **43**, 493 (1960)
47. W.B. Wilson, J. Am. Ceram. Soc. **43**, 77 (1960)
48. A.L. Bowman, G.P. Arnold, W.G. Wittman, T.G. Wallace, N.G. Nereson, Acta. Crystallogr. **21**, 670 (1966)
49. T.B. Massalski, *Binary Alloy Phase Diagrams* (William W. Scott, Jr, Materials Park, Ohio, 1990)
50. B.T.M. Willis, Nature **197**, 755 (1963)
51. D.J.M. Bevan, I.E. Grey, B.T.M. Willis, J. Solid State Chem. **61**, 1 (1986)
52. R.I. Cooper, B.T.M. Willis, Acta Cryst. A **60**, 322 (2004)
53. K. Clausen, W. Hayes, J.E. Macdonald, R. Osborn, M.T. Hutchings, Phys. Rev. Lett. **52**, 1238 (1984)
54. J.P. Goff, B. Fak, W. Hayes, M.T. Hutchings, J. Nucl. Mater. **188**, 210 (1992)
55. G. Dolling, R.A. Cowley, A.D.B. Woods, Can. J. Phys. **43**, 1397 (1965)
56. M.T. Hutchings, J. Chem. Soc. Faraday Trans. **2**, 1083 (1987)
57. J.D. Higgs, W.T. Thompson, B.J. Lewis, S.C. Vogel, J. Nucl. Mater. **366**, 297 (2007)
58. L. Desgranges, G. Baldinozzi, G. Rousseau, J.C. Niepce, G. Calvarin, Inorg. Chem. **48**, 7585 (2009)
59. A.S. Tremsin, J.B. McPhate, J.V. Vallerga, O. Siegmund, J.S. Hull, W.B. Feller, E. Lehmann, Nucl. Instrum. Meth. A **604**, 140 (2009)
60. W.E. Lamb, Phys. Rev. **55**, 190 (1939)
61. Ross AM (1976) Practical applications of neutron radiography and gaging, ASTM STP 586, pp 195–209
62. R. Zboray, J. Kickhofel, M. Damsohn, H.M. Prasser, Nucl. Eng. Des. **241**, 3201 (2011)
63. J.H. Root, C.E. Coleman, J.W. Bowden, M. Hayashi, J. Press Vessel Technol. **119**, 137 (1997)
64. M. Law, O. Kirstein, V. Luzin, J. Strain Anal. **45**, 567 (2010)